Analytical Study of Wind-Tunnel Acoustic Testing of Propellers

Walter Eversman*
University of Missouri-Rolla, Rolla, Missouri 65401

An analytical study based on finite element models is made of the acoustic testing of propellers in a wind-tunnel environment. Features that are considered are the subsonic mean flow, including the effect of a boundary layer; acoustically absorbing wind-tunnel walls; and a lifting line representation of the propeller. The boundary layer is approximated by several layers of uniform mean flow with interlayer boundary conditions forcing continuity of particle displacement. Results are presented as simulated acoustic measurements made at various locations around the propeller in the wind tunnel. Comparisons are made with similar simulated measurements generated by a free-field, finite element model of the same propeller. In the present study, the tunnel Mach number is limited to $M = 0.5$, only purely resistive wall treatment is used, and relatively thick boundary layers are considered. It is found that acoustic pressures near the propeller and removed from the walls compare well with pressures in a free-field environment.

Introduction

THE motivation for the present study is the acoustic testing of model scale propellers in wind-tunnel facilities. It was found in previous investigations[1-3] that, to a considerable degree, it is possible to obtain near-field measurements of both directivity and level, provided the tunnel is acoustically treated and provided that the measurements are not made near the duct wall. The implication is that successful acoustic testing requires the model to be considerably smaller in disk area than the tunnel cross-sectional area.

Previous modeling left unanswered the effect of the boundary layer on the wind-tunnel wall on the success of acoustic measurements. The primary interest here is the effect that the boundary layer has on acoustic measurements both at the wall and at a large distance from the wall.

In this investigation, we consider parameters representative of the testing of an eight-blade advanced turboprop in the NASA Lewis Research Center 8×6 wind tunnel and draw conclusions about the success that can be expected in obtaining acoustic measurements that are representative of free-field measurements, and particularly on the influence of the boundary layer on these measurements. The mathematical model is based on a finite element formulation.

Finite element methods have proven to be effective for solving field equations in a variety of applications in aeroacoustics. Included in recent developments are the modeling of acoustic transmission in ducts without mean flow,[4] transmission in ducts with a nonuniform mean flow,[5] and radiation from duct inlets without[6] and with mean flow.[7,8] These applications have been supported by studies of the fundamental characteristics of the solution methods employed.[9,10] Efficient computer programs using rapid access external disk storage and frontal solution methods[11] have been developed. In these applications, both interior and exterior types of acoustic propagation problems have been addressed.

Ducted propeller noise sources have also been investigated using a direct numerical approach to a lifting line propeller theory, originally presented in analytical form by Gutin.[12] This has involved the extension of finite element modeling techniques to the acoustic field equations with sources and body forces. The result has been models for propeller acoustic radiation in the free-field and in a circular duct wind tunnel.[1-3] In the wind-tunnel case, both rigid walls and acoustically absorptive walls have been considered.[2,3] The work reported here extends the model to include the boundary layer at the wind-tunnel wall. This has been accomplished by approximating the boundary layer, which is a continuous profile from zero velocity at the wall to freestream velocity outside the boundary layer, by a stepped approximation in which the velocity profile is piecewise constant in layers.[13] In the limit of infinitesimally thin layers, the profile of the stepped approximation coincides with that of the continuous profile.

The new model has been incorporated in a computational code originally written for the case when uniform flow is assumed in the wind tunnel. Several innovations in the application of the finite element procedure have been introduced to account for the stepped velocity profile and the particle displacement continuity that must be enforced at the shear-layer interfaces.

Modeling of the Boundary Layer

The model of the propeller in the wind tunnel developed in Refs. 2 and 3 has been expanded to include the effect of the tunnel wall boundary layer. This has been accomplished by using the nondimensional acoustic field equations for sheared flow

$$\frac{\partial p}{\partial t} + M\frac{\partial p}{\partial x} + \nabla \cdot V = 0 \tag{1}$$

$$\frac{\partial V}{\partial t} + M\frac{\partial V}{\partial t} + v_r\frac{\partial M}{\partial r}e_x = -\nabla p + f \tag{2}$$

with suitable wall boundary conditions in the cylindrical duct geometry shown in Fig. 1. The acoustic particle velocity is defined in the cylindrical coordinate system as $V = v_x e_x + v_r e_r + v_\theta e_\theta$. The pressure is scaled by $\rho_0 c^2$, velocity by c, and body force by c^2/R; ρ_0 is the ambient density, c the ambient speed of sound, and R the duct radius. Time is scaled by R/c and lengths by R. The body force per unit mass is used to introduce the propeller loading as described in Refs. 1-3. In Eq. (2), the term $v_r(\partial M/\partial r)\, e_x$ appears because the boundary

Presented as Paper 89-1097 at the AIAA 12th Aeroacoustic Conference, San Antonio, TX, April 10-12, 1989; received June 15, 1989; revision received Jan. 29, 1990.

*Curators Professor, Mechanical and Aerospace Engineering Department.

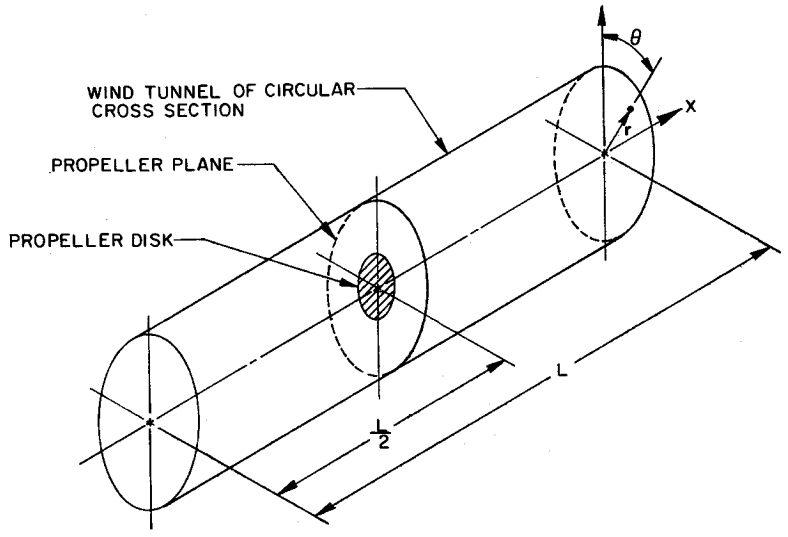

Fig. 1 Geometry of the circular wind tunnel.

layer is assumed to introduce a radial variation of the mean flow Mach number M. The flow is uniform axially.

As is well known, Eq. (1) and (2) can be cast in the form of a sheared flow convected wave equation

$$\frac{D^2p}{Dt^2} - \nabla^2 p + \nabla \cdot f - 2\frac{\partial M}{\partial r}\frac{\partial v_r}{\partial x} = 0 \tag{3}$$

and a subsidiary relation

$$\frac{Dv_r}{Dt} = -\frac{\partial p}{\partial r} \tag{4}$$

with

$$\frac{D}{Dt} = \frac{\partial}{\partial t} + M\frac{\partial}{\partial x}$$

Yet another form can be obtained by combining Eqs. (3) and (4)

$$\frac{D}{Dt}\left[\frac{D^2p}{Dt^2} - \nabla^2 p + \nabla \cdot f\right] + 2\frac{\partial M}{\partial r}\frac{\partial^2 p}{\partial x \partial r} = 0 \tag{5}$$

As discussed in some detail in Ref. 13, [Eqs. (3)–(5)] are not attractive forms for the acoustic field equations because of considerable difficulties and uncertainty anticipated in the finite element model. The ideal model would be one that requires only modest changes in the finite element implementation used when the mean flow is uniform, described in Refs. 2 and 3.

Reference 13 introduced the idea of representing the continuous boundary-layer profile by a stepped approximation in which the velocity is piecewise constant in layers, as shown in Fig. 2. The acoustic field equation reduces to the convected wave equation

$$\frac{D^2p}{Dt^2} - \nabla^2 p + \nabla \cdot f = 0 \tag{6}$$

with the Mach number constant in the core flow and piecewise constant in the boundary layer. In addition, it is required that, at interfaces between layers of uniform flow of different velocity, the condition of continuity of particle displacement be enforced. For the layers j and $j+1$ this condition is

$$\left[\frac{\partial}{\partial t} + M_j\frac{\partial}{\partial x}\right]^2\left(\frac{\partial p}{\partial r}\right)_{j+1} = \left[\frac{\partial}{\partial t} + M_{j+1}\frac{\partial}{\partial x}\right]^2\left(\frac{\partial p}{\partial r}\right)_j \tag{7}$$

Since M_j and M_{j+1} are not equal, the radial pressure gradient must be discontinuous at the N interfaces, $j = 1, \ldots N$.

As shown in Ref. 13, the natural boundary conditions for the finite element formulation of the convected wave equation provide a mechanism for enforcing this condition. It is shown that the weighted residuals formulation in the weak form seeks solutions for the acoustic pressure p from the class of continuous functions that satisfy the requirement that

$$\begin{aligned}\int_\Omega\int\Big[\Big|\nabla W\cdot(\nabla p - e_x M^2 p_x - f) + 2i\eta M W p_x - \eta^2 W p\Big]\\ \times r\,dA + \sum_{j=1}^{N}\int_0^l W\left[\left|\frac{\partial p}{\partial r}\right|\right] r_j\,dx\\ + \int_0^1 W(1-M^2)\frac{\partial p}{\partial x} r\,dr\Big|_{x=0}\\ - \int_0^1 W(1-M^2)\frac{\partial p}{\partial x} r\,dr\Big|_{x=l}\\ - \int_0^l W\frac{\partial p}{\partial r} r\,dr\Big|_{r=1} = 0\end{aligned} \tag{8}$$

for all weighting functions W also chosen from the class of continuous functions. Equation (8) is written for the case of harmonic excitation at the nondimensional frequency $\eta = \omega R/c$. The formulation here has made use of the fact that we treat a specific angular mode for which $p \propto e^{-im\theta}$ and the weighting function is chosen so that $W \propto e^{im\theta}$, reducing the volume integral in the weighted residual to the surface integral over the region Ω in a plane of constant θ in the cylindrical coordinate system. In the present problem, the region Ω is a rectangle (the duct has a uniform cross-sectional area) of length l (nondimensional with respect to the duct radius), which is considered to be the interior region in which the propeller and duct lining are contained. The boundaries $x = 0$ and $x = l$ are the outflow and inflow boundaries (flow is considered in the negative x direction) on which nonreflecting boundary conditions are imposed using the modal matching procedure.[2,3]

In Eq. (8), the jump terms arising from the natural boundary conditions are contained in the summation, where the notation $[|\partial p/\partial r|]$ denotes the jump

$$[|\partial p/\partial r|] = (\partial p/\partial r)_{j+1} - (\partial p/\partial r)_j \tag{9}$$

This is the difference in the radial gradient in pressure above $(j+1)$ and below (j) the shear layer at $r = r_j$.

Equation (7) can be used to determine that

$$\left[\left|\frac{\partial p}{\partial r}\right|\right] = 2i\left[\left(\frac{M_j}{\eta}\right)\frac{\partial}{\partial x}\left(\frac{\partial p}{\partial r}\right)_{j+1} - \left(\frac{M_{j+1}}{\eta}\right)\frac{\partial}{\partial x}\left(\frac{\partial p}{\partial r}\right)_j\right] + \left[\left(\frac{M_j}{\eta}\right)^2\frac{\partial^2}{\partial x^2}\left(\frac{\partial p}{\partial r}\right)_{j+1} - \left(\frac{M_{j+1}}{\eta}\right)^2\frac{\partial^2}{\partial x^2}\left(\frac{\partial p}{\partial r}\right)_j\right] \tag{10}$$

where the derivative $(\partial p/\partial r)_{j+1}$ is to be taken from within the larger $j+1$ and the derivative $(\partial p/\partial r)_j$ is to be taken from within the layer j, both at the radius r_j, which is the interface between the layers for unequal velocity. This gives rise to one of the jump contributions of Eq. (8) at the jth interface.

$$\int_0^l W\left[\left|\frac{\partial p}{\partial r}\right|\right] r_j\,dx = 2i\int_0^l W\left[\left(\frac{M_j}{\eta}\right)\frac{\partial}{\partial x}\left(\frac{\partial p}{\partial r}\right)_{j+1} - \left(\frac{M_{j+1}}{\eta}\right)\frac{\partial}{\partial x}\left(\frac{\partial p}{\partial r}\right)_j\right] r_j\,dx + \int_0^l W\left[\left(\frac{M_j}{\eta}\right)^2\frac{\partial^2}{\partial x^2}\left(\frac{\partial p}{\partial r}\right)_{j+1} - \left(\frac{M_{j+1}}{\eta}\right)^2\frac{\partial^2}{\partial x^2}\left(\frac{\partial p}{\partial r}\right)_j\right] r_j\,dx \tag{11}$$

In principle, these integrals are easily computed in the finite element context. However, the second integral requires a second derivative in x and this has been replaced in the spirit of the weak formulation, which only requires piecewise continuity of first derivatives, by introducing an integration by parts to yield the alternative form

$$\begin{aligned}\int_0^l W\left[\left|\frac{\partial p}{\partial r}\right|\right] r_j\,dx &= 2i\int_0^l W\left[\left(\frac{M_j}{\eta}\right)\frac{\partial}{\partial x}\left(\frac{\partial p}{\partial r}\right)_{j+1} - \left(\frac{M_{j+1}}{\eta}\right)\frac{\partial}{\partial x}\left(\frac{\partial p}{\partial r}\right)_j\right] r_j\,dx \\ &\quad - \int_0^l\left[\left(\frac{M_j}{\eta}\right)^2\frac{\partial W}{\partial x}\frac{\partial}{\partial x}\left(\frac{\partial p}{\partial r}\right)_{j+1} - \left(\frac{M_{j+1}}{\eta}\right)^2\frac{\partial W}{\partial x}\frac{\partial}{\partial x}\left(\frac{\partial p}{\partial r}\right)_j\right] r_j\,dx \\ &\quad + \left(\frac{M_j}{\eta}\right)^2\left\{\left[W\frac{\partial W}{\partial x}\left(\frac{\partial p}{\partial r}\right)_{j+1} r_j\right]_{x=l} - \left[W\frac{\partial}{\partial x}\left(\frac{\partial p}{\partial r}\right)_{j+1} r_j\right]_{x=0}\right\} \\ &\quad - \left(\frac{M_{j+1}}{\eta}\right)^2\left\{\left[W\frac{\partial}{\partial x}\left(\frac{\partial p}{\partial r}\right)_j r_j\right]_{x=l} - \left[W\frac{\partial}{\partial x}\left(\frac{\partial p}{\partial r}\right)_j r_j\right]_{x=0}\right\}\end{aligned} \tag{12}$$

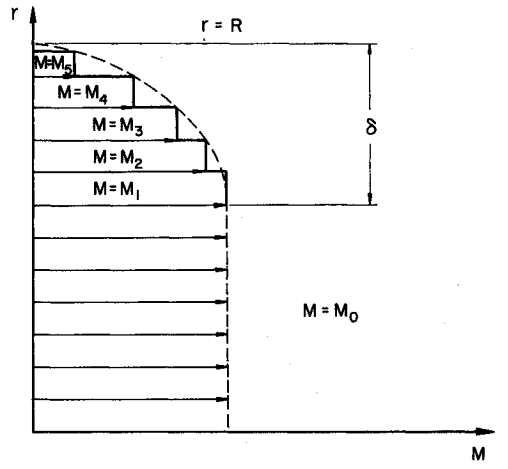

Fig. 2 Approximation of the boundary-layer profile with layers of uniform flow.

The first two integrals are formed along the shear-layer interface at $r = r_j$ and the last two terms are formed on the outflow and inflow boundaries at $x = 0$ and $x = l$. These outflow and inflow boundary terms supplement the two natural boundary conditions on these boundaries described by the integrals on these boundaries in Eq. (8). The boundary condition at the duct outer wall, $r = 1$, is introduced through the final integral of Eq. (8). The use of the natural boundary conditions for modal matching and wall impedance is described in Refs. 2 and 3.

The formulation of Eq. (8) is similar to the formulation for the case with uniform flow described in Refs. 2 and 3, but with the addition of the jump terms, which ultimately introduce contributions to the element stiffness matrices defined by Eq. (12). Implied, but not explicitly stated, is the fact that the natural boundary conditions on $x = 0$ and $x = l$ must be implemented to account for the fact that acoustic modes that include the boundary-layer effect must be used. Certain analytical formulations previously used that took advantage of eigenfunction orthogonality when the flow is uniform are not valid, and the integrals are now evaluated on an element basis rather than globally.[7]

Code Verification

By using the formulation of Eq. (8), a new computer code has been written that includes the boundary-layer approximation described. With the exception of some extra data required to define the boundary-layer profile, the new program appears the same to the user as the old one that was valid only for uniform flow. All aspects of the propeller model[1-3] have been retained unchanged because it is assumed that the propeller is not within the boundary layer. In the region of the duct containing the propeller, the flow is uniform and the original formulation applies.

In Ref. 13, a preliminary assessment of the accuracy of this approximation was made by using it to construct the finite element model for the acoustic eigenfunctions of uniform circular ducts containing a sheared mean flow. When the sheared flow is modeled as a continuous profile, the finite element procedure can also be used to compute accurate eigenvalues that can be used as a baseline against which to check the approximation.[14] In Ref. 13, it was concluded that a good approximation to the acoustic eigenvalues and eigenfunctions can be obtained by using the stepped boundary-layer approximation. In Ref. [13], arguments were also presented for treating the hydrodynamic modes introduced by the shear layers on the same basis as acoustic modes.

A second verification of the approximation concept and the computer code was made by modeling the propagation of an isolated sheared flow duct mode through the unlined duct. For

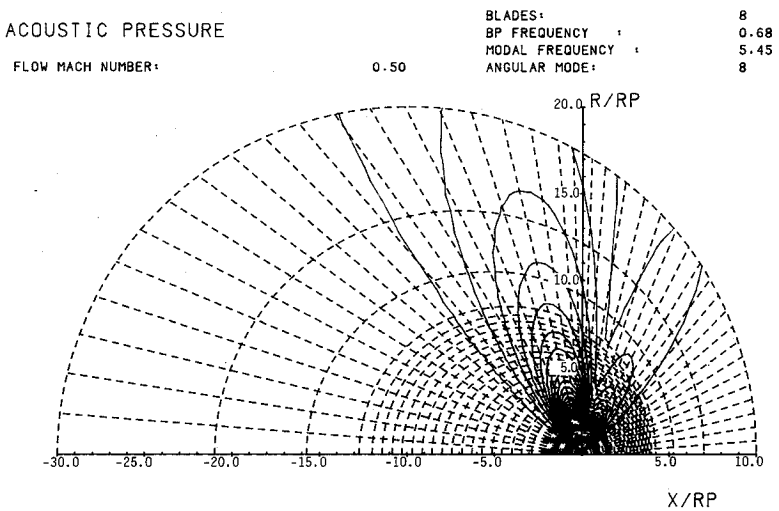

Fig. 3 Contours of sound pressure level in the radiated field for the example propeller (free field).

modes that are cut on, a mode launched with unit amplitude at $x = 0$ should arrive at the far end of the computational region, $x = l$, with unit amplitude. Furthermore, there should be no scattering so that neither reflected modes nor additional propagating modes should appear. As an example, in the case $M = -0.5$, the first radial mode at an angular mode $m = 8$ and frequency $\eta = 21.8$ satisfies all of the required conditions to within scattered modal amplitudes of order 10^{-4}.

Free-Field Calculations

The intent of the present investigation is to assess the degree of success that can be achieved in making acoustic measurements near propeller models in the wind-tunnel environment. Success is defined as the near duplication of results that would be obtained in a true free-field environment. In order to approach this question with the numerical modeling procedure, a free-field representation of the propeller was also constructed to provide the required baseline data. This finite element model is described in Ref. 1.

The propeller considered in this investigation has eight blades with an approximately triangular spanwise load distribution. The propeller radius is $R_p = 1.02$ ft. The propeller speed is 7175 rpm, corresponding to a tip Mach number of $M_{tip} = 0.68125$. The loading is set so that a total thrust of 100 lb is produced. The forward velocity is $M = 0.5$. Based on blade passage frequency and propeller radius, the nondimensional frequency is $\eta = 5.45$. The propeller defined in this way is representative of a model that has been tested in the NASA Lewis Research Center 8×6 wind tunnel.

The results of the free-field calculations are shown in Figs. 3-5. Figure 3 is a plot of lines of constant acoustic pressure magnitude superimposed on the computational grid. Shown here is a plane through the propeller axis, containing the axis X/R_p and any radial axis R/R_p. Both axes are scaled on the propeller radius. The propeller is located near the origin on the R/R_p axis. Note the deformed grid that is an essential feature of the infinite element scheme used to create the far-field radiation boundary condition. This is an essential feature of the finite element model described in Ref. 10. This map of the propeller radiated acoustic field yields a good picture of the directivity that is dominated by a strong lobe behind the propeller disk and a weak lobe ahead of the disk. Figure 4 shows the result of a linear traverse along a line parallel to the X/R_p axis and at a height $R/R_p = 2$, that is at two propeller radii above the propeller axis. This is a near-field sideline directivity that simulates the type of measurements that might be made in the wind tunnel. The scales of this plot require some explanation. The vertical scale is normalized so that the maximum level is 100 dB. The actual maximum level is shown in the legend to be 111.5 dB. The horizontal axis is not scaled by the propeller radius but rather by the radius at which the simulated acoustic measurement is made. This is done to make the comparison of directivities easier in the subsequent discussion. Figure 5 shows a similar sideline directivity obtained at four propeller radii above the propeller. This case will simulate measurements on the wind-tunnel wall. The maximum level for this traverse is 104.3 dB.

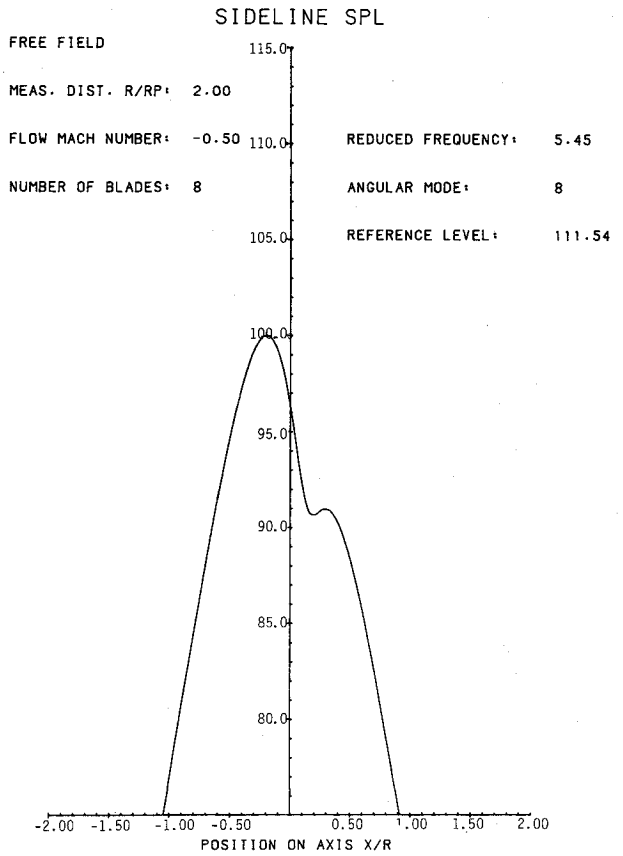

Fig. 4 Sound pressure level on a traverse at two propeller radii from the axis (free field). Axial distance in multiples of measurement radius.

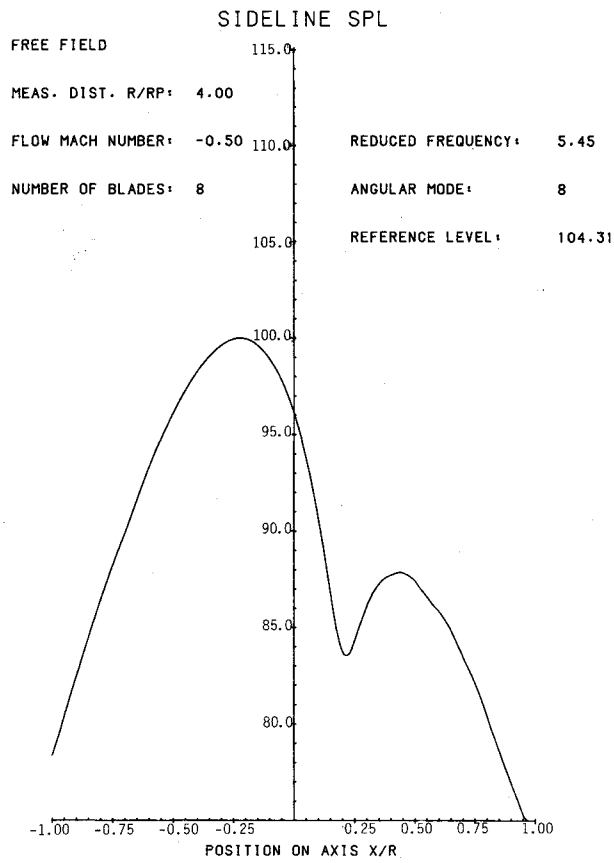

Fig. 5 Sound pressure level on a traverse at four propeller radii from the axis (free field). Axial distance in multiples of measurement radius.

Table 1 Computational examples

Boundary layer	Admittance	Measurement distance, R_m/R_p
$\delta = 0.0$	$A = 0.0$	2.0
		4.0
	$A = 0.9$	2.0
		4.0
$\delta = 0.20$	$A = 0.0$	2.0
		4.0
	$A = 0.9$	2.0
		4.0

Calculations in the Wind-Tunnel Environment

The NASA Lewis Research Center 8×6 wind tunnel is modeled as an equivalent circular tunnel that has a radius four times that of the model propeller, that is $R_d = 4.08$ ft. At the blade passage frequency corresponding to the rotational speed of 7175 rpm for the eight-blade propeller, the nondimensional frequency based on the tunnel radius is $\eta = 21.8$. For the calculations discussed here, the tunnel Mach number is $M = 0.5$, the same as in the free-field calculations. Two simulated measurement radii are considered; one on the tunnel wall and one at two propeller radii from the axis of the tunnel, or one propeller radius from the propeller tip. Acoustic measurements are assumed to be made on a linear traverse at these two radii. Measurements on the tunnel wall are of course made within the boundary layer, whereas those at two propeller radii are well outside the boundary layer.

For this investigation, two boundary-layer situations are considered. In one case, computations are made for uniform flow with no boundary layer. In the other case, a very thick boundary layer of thickness 20% of the duct radius is simulated. The profile is assumed to vary linearly from zero velocity at the wall to the core flow velocity at the edge of the boundary layer. The purpose here is to emphasize the boundary-layer effect. Thinner boundary layers with other profiles are just as easily modeled.

Calculations have been carried out for a range of wind-tunnel wall acoustic treatments applied in a test section that extends one duct radius upstream and downstream of the propeller. In this investigation, only purely resistive linings ranging from vanishing admittance (hard wall) to unity admittance (reflection free for normal incidence) have been considered. This is consistent with the type of acoustic treatment that has been applied in other facilities. In the NASA Lewis 8×6 facility, the walls are not treated specifically for acoustic testing. However, the test section walls are perforated, producing an impedance that is both resistive and reactive. In the present study, this natural acoustic impedance is not considered. The wind tunnel is assumed to be of infinite length so that there are no reflections introduced by bends or due to the closed circuit. However, there are reflections introduced by the transition from hard walls to treated walls in the test section.

In this discussion, eight cases are considered to study the effects of boundary layer, wall treatment, and measurement distance on the quality of acoustic measurements in the wind tunnel. The cases are organized as shown in Table 1.

Figures 6–9 show the radiated acoustic field in the wind tunnel, both without and with the boundary layers, for the two wall admittances. These figures are analogous to Fig. 3 and show contours of constant radiated acoustic pressure

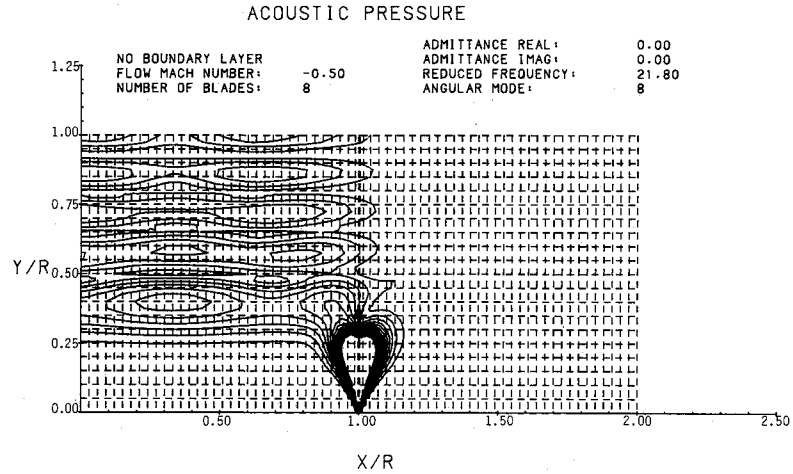

Fig. 6 Contours of sound pressure level in the radiated field for the example propeller in the wind-tunnel environment. Unlined wind tunnel with no boundary layer.

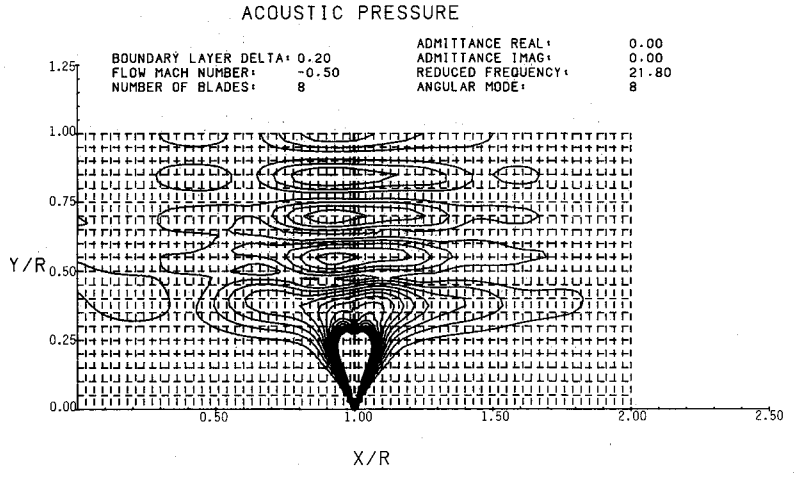

Fig. 7 Contours of sound pressure level in the radiated field for the example propeller in the wind-tunnel environment. Unlined wind tunnel with 20% linear boundary layer.

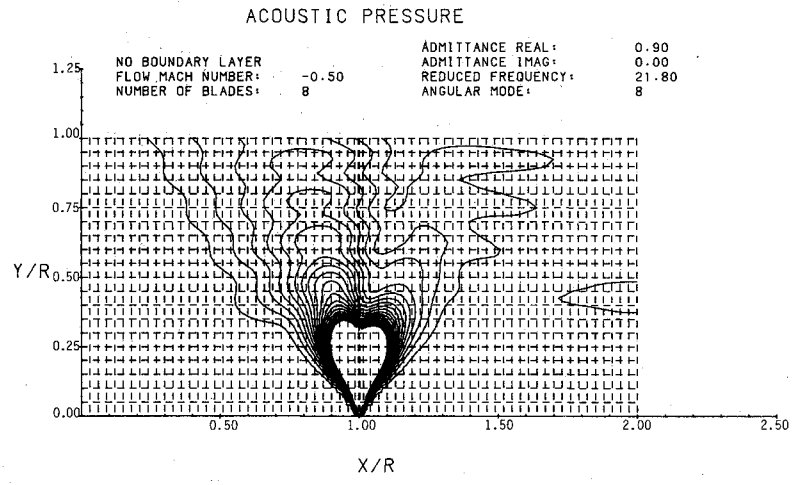

Fig. 8 Contours of sound pressure level in the radiated field for the example propeller in the wind-tunnel environment. Lined wind tunnel with no boundary layer.

amplitude in an X/R, Y/R plane in the cylindrical coordinate system associated with the wind tunnel of circular cross section. Figures 6 and 7 are for the case when the wind-tunnel walls are untreated. When these radiated fields are compared to the free-field pattern of Fig. 3, little similarity can be seen, even near the propeller. Figure 6 shows the radiated field when the boundary layer is absent. There is a strong standing wave pattern above and behind the propeller. The range of contours is chosen to correspond to pressure levels 15 dB above and below the maximum pressure on the wind-tunnel wall. In Fig. 6, it is apparent that the radiation pattern is predominantly behind the propeller. In the case when the boundary layer is present (Fig. 7), there is evidence of a standing wave pattern ahead of the propeller associated with the refractive effect of the boundary layer, which tends to bend acoustic rays traveling upstream away from the duct wall. Figures 8 and 9 show the case when the tunnel wall admittance is $A = 0.90$. It is seen that, in the vicinity of the propeller, a radiation pattern similar to that seen in the free field of Fig. 3 is beginning to emerge. This occurs because of the attenuation of acoustic waves reflected from the duct walls and the resulting reduction in the formation of standing waves. The boundary layer effect is well illustrated in Fig. 9 where it is apparent that ahead of the propeller the effect of boundary-layer refraction has been to push the radiation pattern toward the tunnel axis. These figures provide qualitative evidence that wall treatment enhances the acoustic test environment near the propeller and that the boundary layer tends to reduce the fidelity of the radiated field, particularly ahead of the propeller.

A more quantitative assessment of the effects of boundary layer and wall treatment is shown in Figs. 10 and 11. These figures show simulated acoustic measurements made by traversing a microphone parallel to the duct axis either on the wind-tunnel wall or at a distance of two propeller radii from the duct axis. These two cases are identified by the ratio of the measurement distance to the propeller radius. On the duct wall this is $R/R_p = 4.0$ and near the propeller it is $R/R_p = 2.0$. The horizontal axis is scaled with respect to the measurement radius.

Figures 4 and 5 showed simulated acoustic measurements in the free field. Figure 10 superimposes the free-field measurements at $R/R_p = 4.0$ on those obtained in the duct for the two impedances, both without and with the boundary layer. The most striking observation is that, for untreated tunnel walls, the measurements on the wall compare very poorly with the free-field measurements. In the free field, the maximum sound pressure level (SPL) on the traverse is 104.3 dB, whereas on the wall of the tunnel it is nearly 115 dB. This is noticeably larger than the 6 dB increase one might expect from the blocked pressure effect of normally reflected waves. The explanation for this occurrence is the highly reverberant character of the untreated wind tunnel and the possibility of extended regions in which the acoustic field is reactive. The boundary layer does not strongly affect the peak level but it noticeably shifts the radiation pattern forward and locates the peak magnitude just about in the propeller plane.

When the test section is acoustically treated, the directivity pattern compares much more favorably with the simulated

free-field measurement. The peak level on the tunnel wall is 103.8 without the boundary layer and 103.0 dB with the boundary layer, compared with 104.3 in the free field. The aft radiated lobe is reproduced reasonably well in the absence of boundary layer but is broadened somewhat when the boundary layer is present. The forward lobe is underpredicted as compared to the free field when the boundary layer is absent. The most distinct effect of the boundary layer is the complete suppression of the forward lobe. This is consistent with the refraction effect of the boundary layer that turns acoustic rays away from the duct wall upstream and, hence, should reduce the measured acoustic levels.

Figure 11 shows simulated acoustic measurements taken on the traverse at two propeller radii from the tunnel axis or one propeller radius from the propeller tip. It is noticed that the free-field directivity forms a much narrower peak than when measurements are made at four propeller radii. It is again found that when the duct test section is not acoustically treated the measurements are in poor agreement with the free-field results. In the untreated case, there is a significant difference between the measurements made when the boundary layer is present and when it is absent. The most notable difference is a 5 dB increase in the magnitude of the peak acoustic pressure in the lobe behind the propeller. The

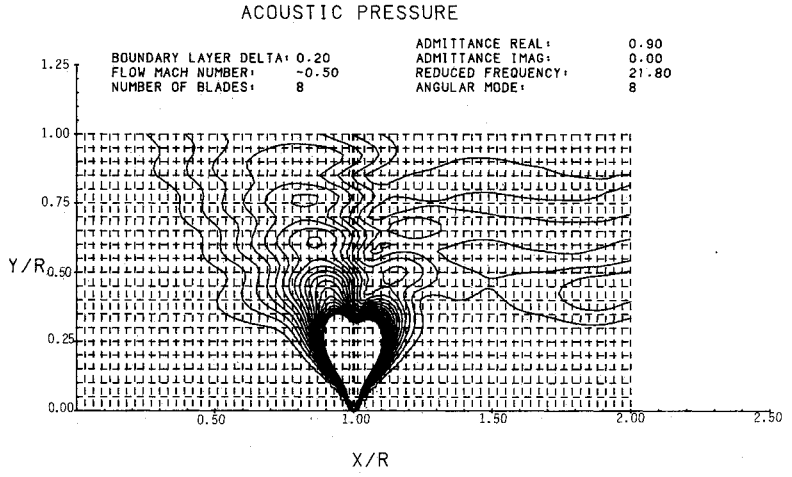

Fig. 9 Contours of sound pressure level in the radiated field for the example propeller in the wind-tunnel environment. Lined wind tunnel with 20% linear boundary layer.

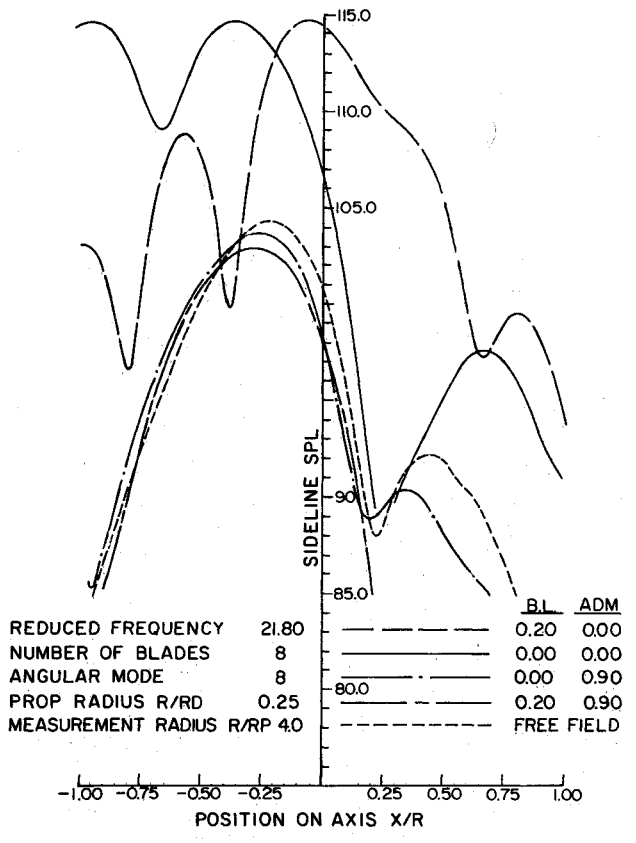

Fig. 10 Composite plot of sound pressure level on a traverse at four propeller radii from the axis. Free field and unlined duct both without and with a boundary layer. Axial distance in multiples of measurement radius.

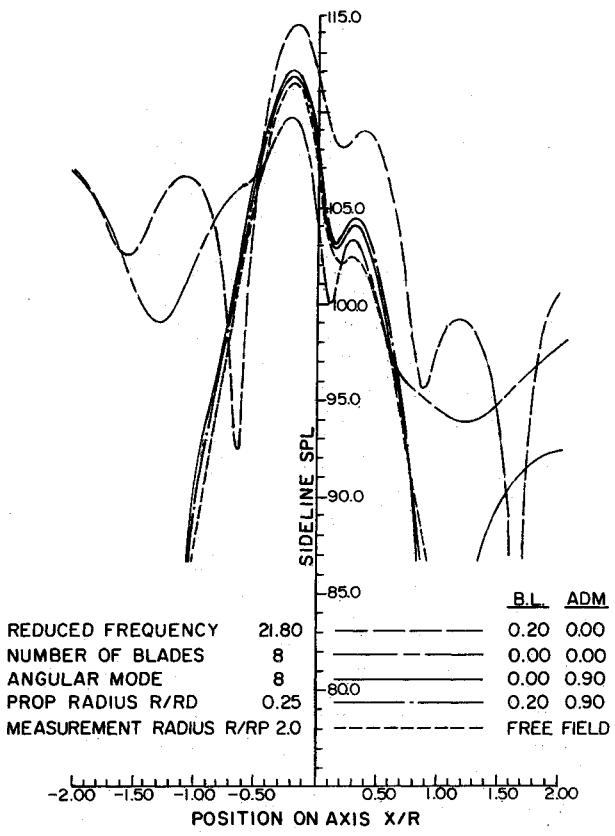

Fig. 11 Composite plot of sound pressure level on a traverse at two propeller radii from the axis. Free field and unlined duct both without and with a boundary layer. Axial distance in multiples of measurement radius.

free-field level in this lobe is 111.5 dB whereas with the untreated walls the level is 109.8 dB when the boundary layer is absent and 114.5 dB when the boundary layer is present. Even though the boundary layer is relatively thick it is difficult to relate this simply to the usual picture of waves refracting into the boundary layer downstream because the measurement radius is well outside the boundary layer. From Figs. 6 and 7 it is concluded that the boundary layer affects the standing wave pattern in a very complex way and it is the pattern created by reflections from the hard wall that makes measurements unreliable.

The picture is quite favorably changed when the test section is treated. As shown in Figure 11, the directivity at two propeller radii when the wall admittance is $A = 0.90 + i0.0$ is a good approximation of the free-field directivity, even to the peak level in the aft radiated lobe. The levels of 112.1 dB in the absence of the boundary layer and 111.9 when the boundary layer is present compare well with the 111.5 dB free-field level. The aft lobe is duplicated well whereas the small forward lobe of considerably lower level is seen in both the free-field and duct measurements, though slightly more pronounced in the duct results. The effect of the boundary layer is minimal, and only appears at very low acoustic levels ahead of the propeller.

There can be little doubt that the best measurement environment of those investigated is near the source in an acoustically treated test section. Under these conditions there is little effect of standing waves and boundary-layer refraction.

Observations and Conclusions

It has been found that an approximation based on the representation of the boundary layer by lamina of uniform flow with appropriate interlayer boundary conditions is accurate and efficient and compatible with finite element formulations. The approximation has been implemented within the framework of existing codes to produce a model with which the acoustic environment in an acoustically treated wind tunnel can be assessed.

A conclusion that can be immediately drawn is that, for the configuration simulated, the untreated test section is not suitable for reliable acoustic measurements. The standing wave pattern that is established by reflection from the wind-tunnel walls is significantly affected by variations in the environment such as introduced by the boundary layer and probably also by other factors such as the characteristics of the source and the tunnel speed. The presence of the strong standing waves makes it highly unlikely that successful comparisons with free-field measurements can be reliably achieved. However, when the wind-tunnel test section is acoustically treated, the standing wave pattern is significantly reduced and, as shown in Figs. 8 and 9, a radiation pattern like the one seen in the free field begins to emerge near the propeller. With the reduction in the standing waves, the sensitivity of the radiated field to disturbances created by the boundary layer is greatly reduced and the success of the measurements becomes nearly independent of the presence of the boundary layer.

In the case of the NASA Lewis 8×6 wind tunnel, there is actually a natural wall admittance associated with pressure relief holes in the test section. At the time of this investigation this had not been quantified; however, actual test results suggest that it is effective in reducing wall reflections and in creating an acceptable environment for measurements.

Acknowledgment

This work was supported by a grant from the NASA Lewis Research Center. The author wishes to express appreciation of the interest and encouragement of John Groeneweg, James Dittmar, and Kenneth Baumeister.

References

[1]Eversman, W., and Steck, J. E., "Finite Element Modeling of Acoustic Singularities with Application to Near and Far Field Propeller Noise," *Journal of Aircraft*, Vol. 23, No. 4, 1986, pp. 275–282.

[2]Eversman, W., and Baumeister, K. J., "Modelling Wind Tunnel Effects on the Radiation Characteristics of Acoustic Sources," *Journal of Aircraft*, Vol. 23, No. 6, 1986, pp. 455–463.

[3]Baumeister, K. J., and Eversman, W., "Effects of Wind Tunnel Wall Absorption on the Acoustic Radiation of Propellers," *Journal of Propulsion and Power*, Vol. 5, No. 1, 1989, pp. 56–63.

[4]Astley, R. J., and Eversman, W., "A Finite Element Method for Transmission in Nonuniform Duct Without Flow: Comparison with the Method of Weighted Residuals," *Journal of Sound and Vibration*, Vol. 57, No. 3, 1978, pp. 367–388.

[5]Astley, R. J., and Eversman, W., "Acoustic Transmission in Nonuniform Ducts with Mean Flow, Part II: The Finite Element Method," *Journal of Sound and Vibration,* Vol. 74, No. 1, 1981, pp. 103–121.

[6]Astley, R. J., and Eversman, W., "Wave Envelope and Infinite Element Schemes for Fan Noise Radiation from Turbofan Inlets," *AIAA Journal*, Vol. 22, No. 12, 1984, pp. 1719–1726.

[7]Eversman, W., Parrett, A. V., Preisser, J. S., and Silcox, R. J., "Contributions to the Finite Element Solution of the Fan Noise Radiation Problem," *Journal of Vibration, Acoustics, Stress, and Reliability in Design*, Vol. 107, No. 2, 1985, pp. 216–223.

[8]Preisser, J. S., Silcox, R. H., Eversman, W., and Parrett, A. V., "A Flight Study of Tone Radiation Patterns Generated by Inlet Rods in a Small Turbofan Engine," *Journal of Aircraft*, Vol. 22, No. 1, 1985, pp. 57–62.

[9]Astley, R. J., Eversman, W., and Walkington, N. J., "Accuracy and Stability of Finite Element Schemes for the Duct Transmission Problem," *AIAA Journal*, Vol. 20, No. 11, 1982, pp. 1547–1556.

[10]Astley, R. J., and Eversman, W., "Finite Element Formulations for Acoustical Radiation," *Journal of Sound and Vibration*, Vol. 88, No. 1, 1983, pp. 47–64.

[11]Irons, B. M., "A Frontal Solution Program for Finite Element Analysis," *International Journal for Numerical Methods in Engineering*, Vol. 2, 1970, pp. 5–32.

[12]Gutin, L., "On the Sound Field of a Rotating Propeller," NASA TM-1195, 1948. (Originally in Russian, 1936)

[13]Everesman, W., and Möhring, W., "A Model of the Wall Boundary Layer for Ducted Propellers," AIAA Paper 87-2742, 1987; also, *Nieuw Archief voor Wiskunde,* Series 4, Vol. 6, No. 1, 1988.

[14]Astley, R. J., and Eversman, W., "A Finite Element Formulation of the Eigenvalue Problem in Lined Ducts with Flow," *Journal of Sound and Vibration*, Vol. 65, July 1979, pp. 61–74.